PHYSICAL REVIEW B **96**, 081113(R) (2017)

Enhancement and interplay of first- and second-order spatial dispersion in metamaterials with moderate-permittivity inclusions

Carlo Rizza,[1,2] Vincenzo Galdi,[3] and Alessandro Ciattoni[2]

[1]*Department of Industrial and Information Engineering and Economics, University of L'Aquila, Via G. Gronchi 18, I-67100 L'Aquila, Italy*

[2]*Consiglio Nazionale delle Ricerche, CNR-SPIN, Via Vetoio 10, I-67100 L'Aquila, Italy*

[3]*Fields & Waves Laboratory, Department of Engineering, University of Sannio, I-82100 Benevento, Italy*

(Received 23 January 2017; revised manuscript received 31 July 2017; published 21 August 2017)

We investigate a class of multilayered metamaterials characterized by moderate-permittivity inclusions and low average permittivity. Via first-principles calculations, we show that in such a scenario, first- and second-order spatial dispersions may exhibit a dramatic and nonresonant enhancement, and may become comparable with the local response. Their interplay gives access to a wealth of dispersion regimes encompassing additional extraordinary waves and topological phase transitions. In particular, we identify a configuration featuring bound and disconnected isofrequency contours. Since they do not rely on high-permittivity inclusions, our proposed metamaterials may constitute an attractive and technologically viable platform for engineering nonlocal effects in the optical range.

DOI: 10.1103/PhysRevB.96.081113

Introduction. Metamaterials are artificial composites of dielectric and/or metallic inclusions in a host medium, which can be engineered so as to exhibit unconventional and/or tailored effective electromagnetic responses. As such, they constitute a unique platform for attaining novel optical mechanisms such as negative refraction, super- and hyperlensing, invisibility cloaking, etc. [1]. In the long-wavelength limit, the metamaterial optical response is typically described in terms of macroscopic phenomenological parameters, such as effective permittivity and permeability [2]. However, if the inclusions are metallic and/or their size is not electrically small, nonlocal effects (i.e., spatial dispersion) may need to be accounted for, e.g., via the appearance of spatial derivatives of the fields in the effective constitutive relationships, or via wave-vector-dependent constitutive parameters [3]. The reader is referred to Refs. [4–8] for a representative sampling of nonlocal homogenization approaches available in the topical literature. It is worth stressing that two cornerstones in metamaterial science, namely, artificial electromagnetic chirality and optical magnetism, are manifestations of first- and second-order spatial dispersion, respectively [9,10]. Artificial electromagnetic chirality [due to three- (3D), two- (2D), and one-dimensional (1D) geometrical chirality [11]] yields interesting phenomena, such as giant optical activity, asymmetric transmission, and a negative refractive index [12]. Artificial or optical magnetism may give rise to a negative refractive index and backward-wave propagation [13].

It is worth noting that second-order spatial dispersion is not fully equivalent to artificial magnetism [14], and this aspect has not been exploited to its fullest extent in applied science. Even though second-order and nonmagnetic nonlocal effects are generally considered to be detrimental for several applications [15], they have been shown to support intriguing phenomena such as the propagation of additional extraordinary waves [16,17] and topological transitions [14,18,19]. Within this context, harnessing these nonlocal effects represents one of the grand challenges of metamaterials science.

Spatial dispersion is essentially ruled by the electrical size $\eta = \Lambda/\lambda$, with Λ denoting a characteristic metamaterial scale (unit-cell size) and λ the vacuum wavelength. Therefore, unlike conventional materials, metamaterials offer a natural way for enhancing nonlocality by tailoring the spatial distribution of the inclusions. There are several strategies to modify the hierarchy of the spatial-dispersion orders: (i) by optimizing the shape and size of inclusions [20], (ii) by exploiting plasmonic resonances [21], (iii) by resorting to extreme regimes where the permittivity and/or permeability are close to zero [11], and (iv) by embedding high-index dielectric inclusions (i.e., with relative permittivity $|\varepsilon_I| \sim 1/\eta^2$) [22,23]. The latter strategy has led to the development of low-loss, all-dielectric metamaterials with electric and magnetic responses [24].

Here, we propose a strategy to enhance both first- and second-order spatial dispersion, so that the effect of their interplay may become comparable with the local response, without resorting to plasmonic resonances. Such an interplay is remarkably unusual in nonresonant scenarios, since first- and second-order spatial-dispersion effects typically differ by orders of magnitude. Moreover, their symmetry properties are also different, since first-order nonlocality is ruled by geometric chirality, whereas second-order nonlocality is not.

We show that the above strategy can be implemented in multilayered metamaterials characterized by *moderate-permittivity* inclusions (MPIs), i.e., with relative permittivity $|\varepsilon_I| \sim 1/\eta$, in conjunction with a relatively low average relative permittivity $\ll 1/\eta$. Via first-principles derivations, we show that transverse magnetic (TM) waves are ruled by a biquadratic, highly tunable dispersion relationship that yields a broad variety of phenomena, encompassing additional extraordinary waves and topological phase transitions. Besides the well-known hyperbolic, elliptic, and mixed regimes, we identify a topologically nontrivial dispersion regime characterized by bounded and multiply connected isofrequency contours accompanied by additional extraordinary waves. The proposed metamaterials, which combine a fairly simple geometrical structure with relaxed (moderate-permittivity) requirements on the material constituents, may provide a versatile and technologically viable platform for dispersion engineering, especially attractive in spectral regions (e.g., optical range) where extremely high-index materials are not available.

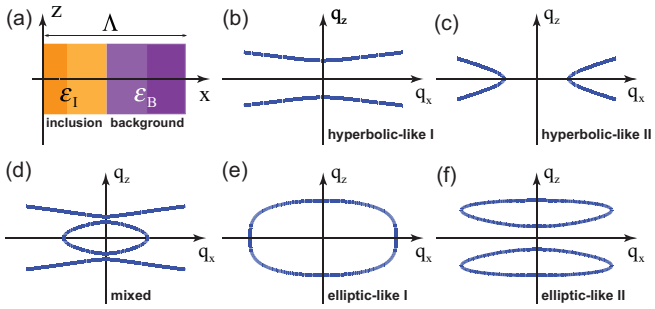

FIG. 1. (a) Schematic of the metamaterial unit cell. (b)–(f) Representative isofrequency contours attainable from Eq. (4).

MPI metamaterials response. With reference to the schematic in Fig. 1(a), we consider a 1D multilayered metamaterial, periodically stratified along the x axis, with a unit cell of thickness Λ consisting of two (possibly composite) regions that we generically indicate as "background" and "inclusion". All fields and quantities are assumed as independent of y, and the metamaterial is described by a piecewise continuous relative permittivity distribution $\varepsilon(x)$, denoted by ε_B and ε_I within the background and the inclusion regions, respectively. In the presence of a monochromatic electromagnetic field (with suppressed $e^{-i\omega t}$ time dependence) whose vacuum wavelength λ is much larger than the unit-cell period, the small ratio $\eta = \Lambda/\lambda$ rules the homogenization of the metamaterial response. As anticipated, we are interested in the MPI regime characterized by the basic requirements

$$|\varepsilon_B| \ll 1/\eta, \quad |\varepsilon_I| \sim 1/\eta, \tag{1a}$$

$$|\overline{\varepsilon(x)}| \ll 1/\eta, \tag{1b}$$

with the overline indicating the average over a unit cell. As detailed in Ref. [25], a rigorous, multiscale analysis of TM-wave (y-directed magnetic field) propagation, in the long-wavelength limit $\eta \ll 1$ and the MPI regime, shows that the leading-order metamaterial response is governed by the effective constitutive relationships

$$\overline{D}_x = \epsilon_0\left(\epsilon_{||}\overline{E}_x + \frac{\kappa}{k_0}\frac{\partial \overline{E}_z}{\partial z}\right), \tag{2a}$$

$$\overline{D}_z = \epsilon_0\left(\epsilon_{\perp}\overline{E}_z - \frac{\kappa}{k_0}\frac{\partial \overline{E}_x}{\partial z} + \frac{\delta}{k_0^2}\frac{\partial^2 \overline{E}_z}{\partial z^2}\right), \tag{2b}$$

$$\overline{B}_y = \mu_0 \overline{H}_y, \tag{2c}$$

with ϵ_0, μ_0, and $k_0 = \omega\sqrt{\epsilon_0\mu_0} = 2\pi/\lambda$ denoting the vacuum permittivity, permeability, and wave number, respectively, and

$$\epsilon_{||} = \left[\overline{\varepsilon^{-1}(x)}\right]^{-1}, \quad \epsilon_{\perp} = \overline{\varepsilon(x)} + \sum_n \frac{A_{-n}A_n}{n^2}, \tag{3a}$$

$$\kappa = i\epsilon_{||}\sum_n \frac{A_{-n}B_n}{n}, \tag{3b}$$

$$\delta = \frac{1}{\epsilon_{||}}\left(\sum_n \frac{A_{-n}A_n}{n^2} - \kappa^2\right) + \sum_{n,m}\frac{A_m A_{-(m+n)}B_n}{m(m+n)}, \tag{3c}$$

where the summations are intended over all integers $n,m \neq 0$, with $n \neq -m$, and A_n/η and B_n are the Fourier coefficients of the functions $\varepsilon(x)$ and $\varepsilon^{-1}(x)$, respectively (with $|A_n|$, $|B_n| \ll 1/\eta$). Equations (2) and (3) summarize the main result of this study, and they show that the MPI regime, in addition to the local response, can exhibit both first- and second-order spatial dispersion. By using the Serdyukov-Fedorov transformation method [9], it can be shown that the obtained first-order spatial dispersion is equivalent to 1D electromagnetic chirality [11], and that the second-order spatial dispersion is nonmagnetic (i.e., there is no transformation yielding a nonvanishing magnetic permeability). It is crucial to stress that Eqs. (2) *do not* contain the small parameter η. From the physical viewpoint, this yields an unprecedented regime where local response and nonlocal effects may interplay at comparable levels. By contrast, in media with shallow dielectric modulation, first- and second-order spatial-dispersion contributions scale as $\sim\eta$ and $\sim\eta^2$, respectively, and hence they are too weak to appear in the leading-order term of the effective response [23].

Our proposed MPI regime in Eqs. (1) forbids the onset of resonances that would produce a dominant local response, and, at the same time, it triggers an anomalous enhancement of nonlocal effects which strengthens (in different ways) the relative weight of standard first- and second-order spatial-dispersion contributions, while leaving higher-order spatial-dispersion contributions at a negligibly weak level. To gain some physical insight into the underlying mechanisms, we start by analyzing the local response. Due to the requirements in Eqs. (1a), the average of $\varepsilon^{-1}(x)$ is dominated by the background contribution ε_B, so that $|\epsilon_{||}| \ll 1/\eta$ [see Eq. (3a)]. This is a key aspect characterizing the MPI regime since, in the presence of a uniformly large dielectric spatial modulation, $|\epsilon_{||}|$ can be exceedingly large so as to yield superlensing effects [28] which are unaffected by spatial dispersion. The requirements in Eqs. (1a), attainable by suitably tailoring the inclusion dielectric profile (see our discussion and examples below), imply that the first contribution $\overline{\varepsilon(x)}$ to $\epsilon_{\perp}$ in Eq. (3a) is not large. Moreover, the Fourier coefficients of $\varepsilon(x)$ (with $n \neq 0$) are A_n/η, with $|A_n| \ll 1/\eta$, and hence $|\epsilon_{\perp}| \ll 1/\eta$. In other words, even if the dielectric modulation is large, the MPI regime is characterized by local effective permittivities that are sufficiently small so as not to overshadow the spatial-dispersion effects. Considering now the nonlocal response, the requirements in Eqs. (1a) imply that all Fourier coefficients of $\varepsilon^{-1}(x)$ are dominated by the background permittivity, and hence $|B_n| \ll 1/\eta$. As a consequence, from Eqs. (3b) and (3c), the strength of the nonlocal response may become comparable with the local one (see also Ref. [25] for a heuristic explanation of the enhancement effects). It is also worth emphasizing that, although the MPI requirements in Eqs. (1) do not explicitly provide indications on the permittivity signs, the most significant spatial-dispersion enhancements [i.e., sizable values of κ and δ in Eqs. (3)] are obtained in configurations mixing positive- and negative-permittivity constituents. From the physical viewpoint, this is not surprising, since these configurations may support surface-plasmon polaritons propagating at the layer interfaces, whose coupling is known to yield strong nonlocal effects [29].

Dispersion relationship for TM waves. In order to illustrate the physical implications of the strong MPI nonlocal response,

we analyze the dispersion relationship of TM waves $H_y = U_y e^{ik_0(q_x x + q_z z)}$, which readily follows from the constitutive relationships in Eqs. (2), viz.,

$$\delta q_z^4 - (\epsilon_\perp + \kappa^2 + \delta\epsilon_{||})q_z^2 - \epsilon_{||}q_x^2 + \epsilon_{||}\epsilon_\perp = 0. \qquad (4)$$

A first important consequence of second-order spatial dispersion (represented by δ) is that such an equation is *biquadratic*. Moreover, the four coefficients in Eq. (4) depend on the four independent effective parameters in Eqs. (3) which, in turn, may assume comparable values. This implies that, in principle, every possible dispersion regime arising from Eq. (4) is accessible. Figures 1(b)–1(f) qualitatively illustrate, in terms of isofrequency contours, the five possible and topologically different dispersion regimes that can be attained: hyperboliclike I and II, mixed, and ellipticlike I and II, respectively. It is remarkable that the relatively simple class of MPI metamaterials is able to support such a variety of dispersion regimes, comprising both bounded [Figs. 1(e) and 1(f)] and unbounded [Figs. 1(b)–1(d)] propagating wave spectra whose isofrequency contours can be either connected [Fig. 1(e)] or disconnected [Figs. 1(b), 1(c), 1(d), and 1(f)]. Elliptic-hyperbolic mixed regimes such as in Fig. 1(d) have been predicted and experimentally observed [14,16,19], together with additional-wave manifestations, in different metamaterial configurations where second-order spatial dispersion plays a key role in the absence of electromagnetic chirality. The distinctive feature of the ellipticlike II regime in Fig. 1(f) predicted in 1D metamaterials is the presence of two propagating waves with the same transverse wave number (i.e., an additional extraordinary wave) within a limited q_x spectral region.

Comparison with full electromagnetic theory. To validate and calibrate the MPI effective model in Eqs. (2), we compare its predictions with rigorous Bloch theory [30] and full-wave numerical simulations [31] (see Ref. [25] for details). As a first illustrative example, we consider a unit cell comprising three homogeneous layers, two of which (labeled as 1 and 2) constituting the inclusion, and the third one (labeled as 3) representing the background [see Fig. 2(a)]. We consider a parameter configuration with $\eta = 0.1$, layer relative permittivities $\epsilon_1 = 3.8$, $\epsilon_2 = -4.2$, and $\epsilon_3 = -0.2$, and filling fractions $f_1 = f_2 = 0.4$ and $f_3 = 0.2$. Such a design fulfills the MPI requirements in Eqs. (1), since $|\varepsilon_B| = 0.2 \ll 1/\eta$, $|\varepsilon_I| \simeq 4 \sim 1/\eta$, and $|\overline{\varepsilon(x)}| = |f_1\epsilon_1 + f_2\epsilon_2 + f_3\epsilon_3| = 0.2 \ll 1/\eta$. For the chosen parameter configuration, we obtain from Eqs. (3) $\epsilon_\perp = -9.2 \times 10^{-2}$, $\epsilon_{||} = -1$, $\kappa = -0.41$, and $\delta = 3.4 \times 10^{-3}$. This yields the ellipticlike II dispersion regime in Fig. 1(f), where additional waves are expected, as sketched in Fig. 2(a). Figure 2(b) compares the isofrequency contours computed from Eq. (4) with the Bloch-theory [30] solution. A fairly good agreement is evident, as well as the occurrence of an additional extraordinary wave, which is accurately captured by the MPI effective model. Note also that $\overline{\varepsilon(x)} = -0.2$ and $[\overline{\varepsilon^{-1}(x)}]^{-1} = -1$, so that the standard (local) effective-medium theory (EMT) [1] predicts that plane-wave propagation is forbidden (evanescent) in the medium, in stark contrast with the above evidence. It is worth stressing that, in contrast to high-index-inclusion metamaterials [22], such a regime dominated by spatial dispersion is accessed here by means of *moderate* values of the layer permittivities. As

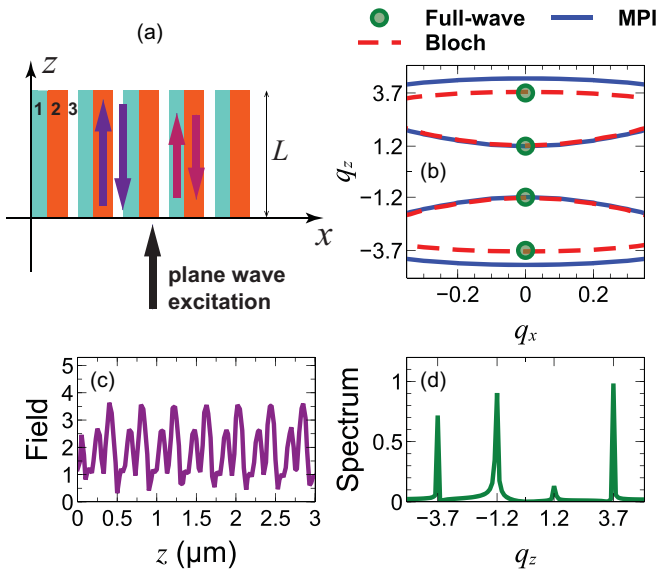

FIG. 2. First example (details in the text). (a) Schematic of the MPI metamaterial slab, and excitation of additional extraordinary waves (thick arrows). (b) Comparison among the isofrequency computed via the MPI effective model (blue solid curves), Bloch theory (red dashed curves), and full-wave simulations (only for $q_x = 0$, green circle markers). (c) Magnitude distribution of the average magnetic field $|\bar{H}_y(z)|$, normalized by the incident field. (d) Corresponding spatial spectrum (magnitude), in arbitrary units.

a further validation check, we also analyzed via full-wave simulations a MPI metamaterial slab of thickness $L = 10$ μm, with the above parameters and period $\Lambda = 0.1$ μm, under normally incident (along z) plane-wave illumination with wavelength $\lambda = 1$ μm [see Fig. 2(a)]. Figure 2(c) shows the magnitude of the average field distribution $|\bar{H}_y(z)|$, whose standing-wave pattern reveals the occurrence of different spatial harmonics. This is more evident in the corresponding spatial spectrum (magnitude) shown in Fig. 2(d), which displays four distinct peaks corresponding to two forward- and two backward-propagating waves, thereby proving the actual excitability of additional extraordinary waves in a finite-thickness slab. For a more quantitative assessment, the normalized wave numbers q_z corresponding to the spectral peaks are superimposed (circle markers) on the isofrequency contours in Fig. 2(b), showing a good agreement with those predicted by the above description of an unbounded MPI metamaterial.

Further details on the range of applicability of our proposed MPI homogenization scheme can be found in Ref. [25].

Topological transitions. The existence of various different dispersion regimes implies that MPI metamaterials may also host unusual topological transitions. As a second representative example, we consider a three-layer unit cell of period $\Lambda = 0.05$ μm, with material constituents chosen as silver (labeled as 1, and playing the role of the inclusion), silicon dioxide (SiO_2), and air (labeled as 2 and 3, respectively, and playing the role of the background), with filling fractions $f_1 = 0.15$, $f_2 = 0.33$, and $f_3 = 0.52$. For silver, we utilize the Drude model $\epsilon_1 = \epsilon_b - \omega_p^2/(\omega^2 + i\alpha\omega)$ (with $\epsilon_b = 5.26$,

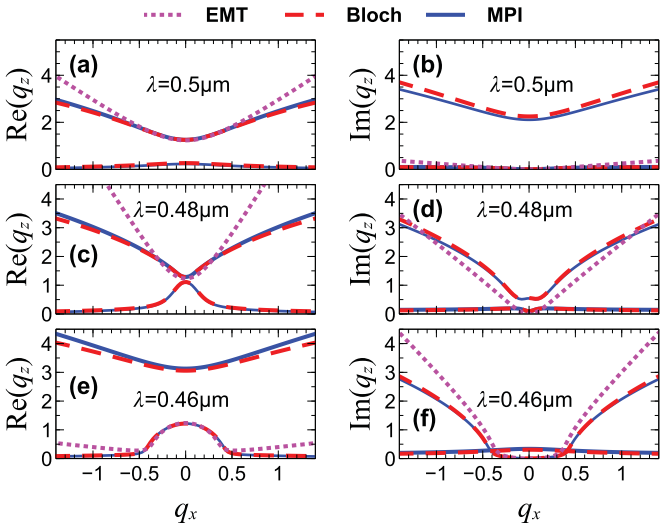

FIG. 3. Second example (details in the text). Complex isofrequency contours at three representative wavelengths (indicated in the panels), computed via the MPI effective model (blue solid curves), Bloch theory (red dashed curves), and EMT (magenta dotted curves). Due to symmetry, only the branches pertaining to forward-propagating waves are shown.

$\alpha = 7.06 \times 10^{13}$ s^{-1}, $\omega_p = 1.45 \times 10^{16}$ s^{-1} [32]), whereas for SiO_2 (ϵ_2) we employ an empirical Sellmeier equation [33]. Figure 3 shows the complex isofrequency contours (real and imaginary parts of q_z as a function of q_x), at three representative wavelengths $\lambda = 0.5$, 0.48, and 0.46 μm for which the MPI requirements in Eqs. (1) are fulfilled. Once again, the agreement between the MPI effective model and Bloch theory is remarkably good at any wavelength, whereas the EMT provides an inadequate description, as it captures only a portion around $q_x = 0$ of a single connected component of the isofrequency contours. Note that, at $\lambda = 0.5$ μm, the dispersion is of hyperboliclike I type, since the additional branches [lower in Fig. 3(a), and upper in Fig. 3(b)] are generated by the presence of loss (they disappear in the lossless limit). On the other hand, at $\lambda = 0.46$ μm [Figs. 3(e) and 3(f)], a mixed regime is observed, and this indicates that a topological transition between the two regimes occurs. As also observed in Ref. [18], such a transition is accompanied by an intermediate state at $\lambda = 0.48$ μm [see Figs. 3(c) and 3(d)] where the two dispersion branches of the mixed regime merge at $q_x = 0$, thereby yielding a wave-vector degeneracy and an associated Dirac point.

Conclusions. In conclusion, we have introduced a class of 1D MPI metamaterials that may exhibit an anomalous electrodynamic behavior driven by nonlocal effects. By comparison with other strategies for spatial-dispersion enhancement, our proposed framework relaxes the requirements on the refractive index of the inclusions, by affording moderate values. In essence, the specific structure of the MPI requirements in Eqs. (1) crucially alters the hierarchy of spatial-dispersion orders, leading to an interplay between first- and second-order nonlocal effects, whose strength may become comparable with the local response. This in turns leads to a variety of different dispersion regimes supporting exotic phenomena such as topological phase transitions and additional extraordinary waves. In view of their technological viability and potential versatility, we believe that MPI multilayered metamaterials, and their possible higher-dimensional extensions, may play a pivotal role for conceiving different platforms for dispersion-engineering applications over a broad electromagnetic spectrum, including the optical range.

Acknowledgments. C.R. and A.C. thank the US Army International Technology Center Atlantic for financial support (Grant No. W911NF-14-1-0315). This work has been supported by the CNR-SPIN Seed Project No. B52F17001370005.

[1] W. Cai and V. Shalaev, *Optical Metamaterials: Fundamentals and Applications* (Springer, Dordrecht, 2010).
[2] D. R. Smith, S. Schultz, P. Markos, and C. M. Soukoulis, Phys. Rev. B **65**, 195104 (2002).
[3] L. D. Landau and E. M. Lifshitz, *Electrodynamics of Continuous Media* (Pergamon, New York, 1960).
[4] M. G. Silveirinha, Phys. Rev. B **75**, 115104 (2007).
[5] J. Elser, V. A. Podolskiy, I. Salakhutdinov, and I. Avrutsky, Appl. Phys. Lett. **90**, 191109 (2007).
[6] A. Alù, Phys. Rev. B **84**, 075153 (2011).
[7] A. V. Chebykin, A. A. Orlov, A. V. Vozianova, S. I. Maslovski, Y. S. Kivshar, and P. A. Belov, Phys. Rev. B **84**, 115438 (2011).
[8] A. V. Chebykin, A. A. Orlov, C. R. Simovski, Y. S. Kivshar, and P. A. Belov, Phys. Rev. B **86**, 115420 (2012).
[9] A. N. Serdyukov, I. V. Semchenko, S. A. Tretyakov, and A. Sihvola, *Electromagnetics of Bi-Anisotropic Materials: Theory and Applications* (Gordon and Breach, Amsterdam, 2001).
[10] A. Ciattoni and C. Rizza, Phys. Rev. B **91**, 184207 (2015).
[11] C. Rizza, A. Di Falco, M. Scalora, and A. Ciattoni, Phys. Rev. Lett. **115**, 057401 (2015).
[12] Z. Li, M. Mutlu, and E. Ozbay, J. Opt. **15**, 023001 (2013).
[13] D. R. Smith, W. J. Padilla, D. C. Vier, S. C. Nemat-Nasser, and S. Schultz, Phys. Rev. Lett. **84**, 4184 (2000).
[14] M. A. Gorlach and P. A. Belov, Phys. Rev. B **90**, 115136 (2014).
[15] A. Demetriadou and J. B. Pendry, J. Phys.: Condens. Matter **20**, 295222 (2008).
[16] R. J. Pollard, A. Murphy, W. R. Hendren, P. R. Evans, R. Atkinson, G. A. Wurtz, A. V. Zayats, and V. A. Podolskiy, Phys. Rev. Lett. **102**, 127405 (2009).
[17] A. A. Orlov, P. M. Voroshilov, P. A. Belov, and Y. S. Kivshar, Phys. Rev. B **84**, 045424 (2011).
[18] A. A. Orlov, A. K. Krylova, S. V. Zhukovsky, V. E. Babicheva, and P. A. Belov, Phys. Rev. A **90**, 013812 (2014).
[19] M. S. Mirmoosa, S. Y. Kosulnikov, and C. R. Simovski, Phys. Rev. B **92**, 075139 (2015).
[20] E. Saenz, I. Semechenko, S. Khakhomov, K. Guven, R. Gonzalo, E. Ozbay, and S. Tretyakov, Electromagnetics **28**, 476 (2008).
[21] I. D. Leon, M. J. Horton, S. A. Schulz, J. Upham, P. Banzer, and R. W. Boyd, Sci. Rep. **5**, 13034 (2015).

[22] D. Felbacq and G. Bouchitté, Phys. Rev. Lett. **94**, 183902 (2005).
[23] R. Merlin, Proc. Natl. Acad. Sci. USA **106**, 1693 (2009).
[24] A. Krasnok, R. Savelev, D. Baranov, and P. Belov, arXiv:1610.05363.
[25] See Supplemental Material at http://link.aps.org/supplemental/10.1103/PhysRevB.96.081113 for a description of the homogenization theory, its range of applicability, a heuristic interpretation of the spatial-dispersion enhancement effects, and some details on the numerical simulations, which includes Refs. [26,27].
[26] M. Born and E. Wolf, *Principles of Optics*, 7th ed. (Cambridge University Press, Cambridge, UK, 1999).
[27] M. Kraft, A. Braun, Y. Luo, S. A. Maier, and J. B. Pendry, ACS Photon. **3**, 764 (2016).
[28] C. Rizza and A. Ciattoni, Phys. Rev. Lett. **110**, 143901 (2013).
[29] O. Kidwai, S. V. Zhukovsky, and J. E. Sipe, Phys. Rev. A **85**, 053842 (2012).
[30] J. D. Joannopoulos, S. G. Johnson, J. N. Winn, and R. D. Meade, *Photonic Crystals: Molding the Flow of Light* (Princeton University Press, Princeton, NJ, 2011).
[31] COMSOL Group, *COMSOL Multiphysics: Version 3.4* (COMSOL, Stockholm, 2008).
[32] P. B. Johnson and R. W. Christy, Phys. Rev. B **6**, 4370 (1972).
[33] I. H. Malitson, J. Opt. Soc. Am. **55**, 1205 (1965).